Filamentation effects and second-harmonic spectra in laser-produced plasmas

A. H. Khalfaoui, S. Abdelli, T. Kerdja, and D. Ghobrini
MDRTE, Centre de Développement des Technologies Avancées 2, boulevard Frantz Fanon, Alger-gare, Boîte Postale 1017, Alger 16000, Algeria
(Received 14 August 1992)

Sideway scattered second-harmonic spectra emitted from a 1064-nm-laser-produced plasma have been observed to originate from nonlinear coupling near the critical surface. The time evolution of the second-harmonic optical density confirmed the possibility that a plasmon issued from the resonant absorption of the incident beam can recombine with a photon (ω_0) to give a transverse wave of frequency $2\omega_0$. A plasmon issued from a parametric decay instability may also, by coalescence with an incident photon, give a transverse wave at a shifted second-harmonic frequency. The threshold of such a combination is determined. Moreover, irregular plasma-parameter variations and the perturbed spatial uniformity of the incident beam appear to alter the second-harmonic spectra. An oscillatory structure of the optical density of the observed second harmonic is interpreted as a result of the coupling physics involved and of laser-beam filamentation.

PACS number(s): 52.40.Nk, 52.35.Nx, 52.25.−b

I. INTRODUCTION

Spectroscopy of 2ω light generated through sum frequency originating from linear (resonant absorption), as well as nonlinear processes in a inhomogeneous plasma, can be a powerful tool to diagnose the laser-plasma interaction. It has the same diagnostic capability as the spectroscopy of Brillouin backscattering light. The latter can be used to measure the electron temperature and estimate the plasma turbulence and related parameters. The second-harmonic light can give, in addition to the same sort of information, more insight into the behavior of the laser-beam structure.

It has been mainly studied in the presence of a critical density layer where its generation is far more probable, [1–3]. Only a few works report on the observation of 2ω emission from undercritical plasma [4]. The mechanism of such generation and information on the plasma parameters that can be obtained are completely different in the two cases.

We report here on spectroscopic studies of second-harmonic light emission from plasma produced by 1.064-μm irradiation of planar targets. The observations and the analysis show that the 2ω emission results from both linear and nonlinear laser-plasma-interaction mechanisms near the critical density (n_c).

There are two main interaction processes that contribute to 2ω emission: resonant absorption, which involves linear conversion of incident photons into Langmuir waves at n_c and the parametric decay instability (PDI), in which the incident electromagnetic wave decays into a Langmuir wave and an ion acoustic wave just below n_c. Qualitatively, the latter possibility of exciting longitudinal oscillation arises at a sufficiently high density of laser radiation energy flux, where parametric instabilities develop at certain thresholds. This situation has been well studied in Ref. [5]. Our results serve to confirm these origins and to extend the investigation of the coupling physics.

The present understanding of the physical essence of the phenomenon of second-harmonic generation has revealed new possibilities of laser-plasma diagnostics. Analysis of the spectrum can provide information about laser-beam behavior [6]. As the photon beam impinges on the critical surface to create the harmonic, its structure is altered by filamentation. It self-focuses, develops substructures, and collapses into a number of filaments [7,8].

Filamentation instability in laser-produced plasmas is of great interest because of its possible role in degrading the coupling of lasers to inertial confinement fusion targets. Filaments have been invoked to explain numerous experimental phenomena, one of which is the observation of emission at the second harmonic of the laser frequency from underdense plasma at angles perpendicular to the incident laser beam [9]. However, no direct link between filaments and this emission has been demonstrated to date. In the present analysis, one of our tasks is to find such a link between the second-harmonic-generation spectrum behavior and the laser-beam spatial structure.

This type of relation is mainly due to the origin of the 2ω generation which is formally stated as follows: The generation of a transverse electromagnetic wave of frequency 2ω in such a plasma is possible only if at least one of the combining waves is a longitudinal oscillation (l) with frequency ω whose value is equal or near to the frequency of the transverse wave [5,10]. The processes which are then possible, of coalescence of a transverse wave t with a longitudinal Langmuir oscillation l to form a transverse wave t, or coalescence of two Langmuir oscillations l into a transverse wave t can be written in the form

$$t+l\rightarrow t\ ,\quad l+l\rightarrow t\ .$$

In a weakly inhomogeneous plasma the wave vector still depends on the coordinates, so that the phase-matching condition $\mathbf{k}=\mathbf{k}'+\mathbf{k}''$ is satisfied only at certain surfaces in space. If there are no such points on the

 ©1993 The American Physical Society

electron-density profile, then the probability of the effect is exponentially small [10].

The second-harmonic intensity is proportional to the energy fluxes of the waves involved in its production and is significant only when the intensity levels of the electron Langmuir oscillation and the transverse waves are high enough. Furthermore, any process which should come to perturb or alter the Langmuir spectrum near the critical density should be clearly observed on the second-harmonic spectra since at least one Langmuir wave is involved in the recombination process.

Strong Langmuir turbulence, where localized Langmuir wave packets have energy densities several orders of magnitude higher than the average energy density [11] and are extremely dynamic before collapsing, has an observed effect on the second-harmonic spectra [12]. Laser bandwidth has been observed to have an effect on the coupling physics [7]. Similarly, any variation of the incident-beam density, such as an anomalous local intensification like the phenomena of filamentation, should have its effect on the second-harmonic spectra behavior.

Some evidence of such effects will be presented in the present analysis. This work is organized as follows: First the experimental arrangement will be described briefly. Then, in order to confirm the origin of the second-harmonic generation, an analysis of the time-integrated spectra will be presented. The optical density of this harmonic, being very sensitive to all effects related to its production, will be studied as time dependent in connection with the critical surface motion and Doppler shifts. The coupling physics will be treated by a simple analytical model to correlate plasma parameters to the second-harmonic behavior and their eventual relations with the impinging laser-beam instability.

II. EXPERIMENTAL ARRANGEMENT

In the present experiment, a plasma was produced by focusing a Nd:YAG (where YAG denotes yttrium aluminum garnet) laser pulse of $\tau_0=0.7$ nsec with a wavelength of $\lambda_0=1.064$ μm through a $f/1.2$ lens on a slab target of polyethylene $(CH_2)_n$. The intensity range used was such that

$$7.0\times10^{12}<I_0<3\times10^{14}\ \mathrm{W/cm^2}\ ,$$

with an incident angle $0°<\theta<11.7°$. The focal spot receiving the 80% of the incident energy was measured and has a value $d=(22\pm4)$ μm, i.e., $d\approx20\lambda_0$.

The sidescattered 2ω spectra were observed at about 45° with respect to the p-polarized incident beam (Fig. 1). Using a 1200-lines/mm, 1-m-long spectrograph coupled to a streak camera (Imacon 675), the time evolution of the 2ω spectra have been recorded.

An image of the target is accurately focused at the entrance slit of the spectrograph. The output plane of the spectrograph is then imaged on the entrance slit of the streak camera. In order to obtain λ-t photograph, it was necessary for the images of the spectrograph slit and the streak camera slit to be at a right angle. To obtain a good resolution, the spectrograph–streak-camera distance was chosen such that the dispersion on the screen was about 10 Å/mm. The spectrograph–streak-camera combination was calibrated using a mercury arc lamp, a HeNe laser, and a frequency-doubled Nd:YAG laser.

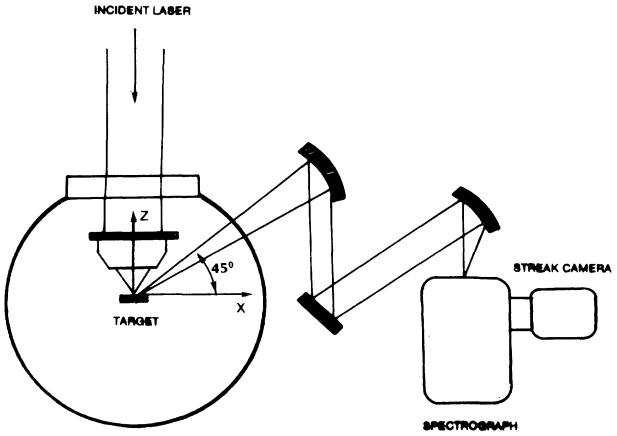

FIG. 1. Experimental setup showing the main elements used for the detection of the second harmonic at 45° and the incident beam normal to the target.

The overall time resolution of the streak camera is limited by two factors: the first due to the camera itself and the second resulting from the temporal broadening in the spectrograph which is given by the maximum difference between the transit time of light incident at different parts of the grating and the output plane of the spectrograph. The amount of grating filled was approximately 0.8 cm, giving a time resolution of 16 psec. The instrumental time resolution of the camera is given by the manufacturer and for our working conditions it is about 2 psec. The spectrograph slit was set to 40 μm and the camera slit was set to 50 μm. The slit width of the spectrograph is near the diffraction limit of the system, so it will be the same at the output plane of the spectrograph. The magnification from the output plane of the spectrograph to the camera screen was three times, giving a spectral resolution of 0.4 Å and a temporal resolution of 3 psec. From the temporal broadening of the spectrograph, the absolute limit on the spectral resolution given by the incertainty principle is 0.6 Å, so the temporal resolution is estimated to be 16 psec and the spectral resolution, 0.6 Å.

A microdensitometer has been used to measure the optical density from the photographic films with dynamic range of over two orders of magnitude. The microdensitometer resolution was set to 1 Å and 15 psec. The bandwidth of laser beam used was estimated to be much less than any wavelength measured value.

III. SECOND-HARMONIC SPECTRA

A. Time-integrated 2ω spectra

These spectra present a general structure with a main peak and one or more secondary peaks, depending on the incident flux intensity. At a given incident flux (Fig. 2),

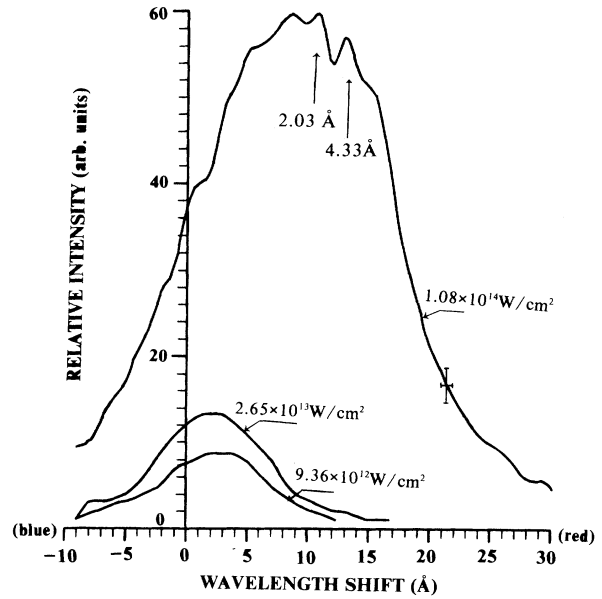

FIG. 2. Time-integrated spectra of the second-harmonic relative intensity as a function of the wavelength shift distinctly showing the main peak and the two satellites peaks at an incident flux of 1.08×10^{14} W/cm^2. For lower fluxes (2.65×10^{13} W/cm^2 and 9.36×10^{12} W/cm^2), no peaks can be distinguished and the main peaks are less shifted.

the main peak is produced through the scattering of incident photons off electron waves generated by resonance absorption giving 2ω light [2,3].

The secondary peaks are quite distinct and better resolved at relatively higher fluxes (Fig. 2, 1.08×10^{14} W/cm^2) than those obtained at lower fluxes (Fig. 2, 2.65×10^{13} and 9.36×10^{12} W/cm^2) where the spectrum is less shifted and no secondary peaks can be distinguished.

Moreover, the main peaks are slightly redshifted from the nominal 5320 Å, due to the Doppler effect associated with the critical density motion (resonance region). These observed shifts are flux dependent, confirming their relation to the critical surface motion through the Doppler effect.

Since the process of linear conversion of light into longitudinal waves is possible in an inhomogeneous plasma near the plasma resonance in the presence of an incident wave whose electric-field vector component is directed along the density gradient, second-harmonic radiation is emitted from such a system where Langmuir waves and light waves are both present. The harmonic frequency so generated is shifted in the presence of motion of the critical surface as follows [13]:

$$\omega_2=2\omega_0-2(\mathbf{k}_0-k_0\mathbf{z})\cdot\mathbf{u} .$$

$\mathbf{u}$ is the critical surface velocity. The shift relative to the nominal value of $2\omega_0$ will be in the blue or the red direction, depending on whether the critical density surface moves towards ($u>0$) or away ($u<0$) from the beam.

The maximum value of the shift is attained when the pump wave is incident along the direction of the divergence of the plasma, i.e.,

$$\mathbf{k}_0=-k_0\mathbf{z} \quad \text{or} \quad \Delta\omega=4\omega_0 u/c .$$

Moreover, the change in the velocity u during the time of registration of the harmonic should lead to additional broadening of the spectrum for a sufficiently long time of exposure.

The first secondary peak indicates that parametric decay instability produces electron waves, from which two plasmons, each of frequency $\omega_{EP}=\omega_0-\omega_{IA}$, are combined to generate 2ω light with a frequency shift $\Delta\omega=2\omega_{IA}$. Since this generation mechanism is viewed as the inverse of the two-plasmon decay instability with a large wavenumber component perpendicular to ∇_n, the emission should be largest near 45° with respect to the incident laser axis [14], as the present detection was conducted.

The second satellite peak in Fig. 2, at 1.08×10^{14} W/cm^2, has exactly twice the shift of the first peak. An interpretation of this observation has been proposed in Ref. [5]; it seems consistent with the present experimental results and will be generalized here.

Electron decay instability (EDI) has a very low threshold [15], and when an electron plasma wave (ω_{EP}) from the primary PDI decays into a new electron wave (ω'_{EP}) and an ion acoustic wave (ω_{IA}) through EDI, these new electron waves may combine with any other plasmon present at the phase-matching point, giving rise to a shifted 2ω light.

As a rule, the combination of two plasmons from PDI gives rise to a peak with a frequency shift equal to $2\omega_{IA}$; if one plasmon originates from PDI and the other from EDI, the harmonic peak so generated will be redshifted by $4\omega_{IA}$ with respect to ω_0, and if both plasmons take their origin from EDI, the peak of such generation will be shifted by $6\omega_{IA}$.

Moreover, in the presence of such a turbulent Langmuir spectrum, further peaks with shifts, regularly spaced, equal to $2n\omega_{IA}$, n integer, can be expected. In Fig. 3, optical density as a function of the wavelength shift is shown. Secondary peaks regularly spaced with $2n\omega_{IA}$ shifts are clearly distinguished at an incident flux of 1.08×10^{14} W cm^{-2}.

However, for higher incident flux (3×10^{14} W cm^{-2}) where no secondary peaks can be seen, this mechanism is likely to be responsible for the broadening of the spectrum. The shifted peaks which are rather narrowly spaced (not well resolved) get to a level comparable to the primary peak and contribute to the widened spectrum.

From energy and momentum conservation and the dispersion relations of the waves involved in these mechanisms, shifts can be evaluated from ion acoustic frequency. In the present experiment, the laser was focused through an incident cone of $\theta=11.7°$ so the density the photons can reach is $n_e(z)=n_c\cos\theta$, to which corresponds an ion frequency of

$$\omega_{IA}=\tfrac{1}{3}^{1/3}\omega(Zm_e/m_i)^{1/2}\sin\theta , \quad (1)$$

and the wavelength shift related to this frequency is

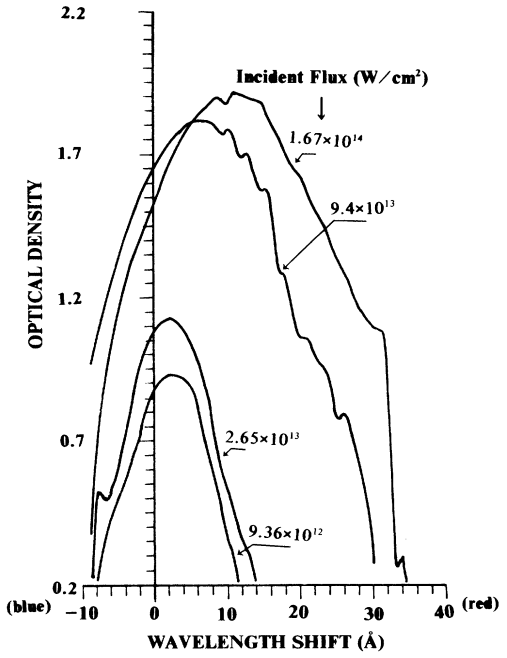

FIG. 3. The time-integrated spectra represent the optical density as the wavelength shift. Several secondary peaks with $2n\omega_{IA}$ shifts are observed at 9.4×10^{13} W/cm^2. For the incident flux around the PDI threshold and below, in the optical density of the second harmonic, no secondary peaks are expected and the main peaks are again relatively less shifted. For higher incident flux (1.67×10^{14} W/cm^2), the Langmuir spectrum is turbulent and the electron decay instability has an important contribution to the second harmonic which makes the time-integrated optical density spectrum broaden with a relatively higher amplitude.

$$\Delta\lambda=(\lambda/2\sqrt{3})(Zm_e/m_i)^{1/2}\sin\theta\ . \tag{2}$$

Then the range in which shifts are included should be as follows: $0\ \text{Å}<\Delta\lambda<12\ \text{Å}$.

Shifts at different fluxes have been measured; they are all included in this interval and are shown in Table I.

Secondary peak components attributed to PDI have a theoretical threshold [16] which can be written as

$$[I_{\text{th}}^{\text{PDI}}\ (\text{W/cm}^2)] =3\times10^{11}\{[T\ (\text{eV})]/[\lambda_\mu\ (\mu\text{m})]^2[L_\mu\ (\mu\text{m})]\}\ , \tag{3}$$

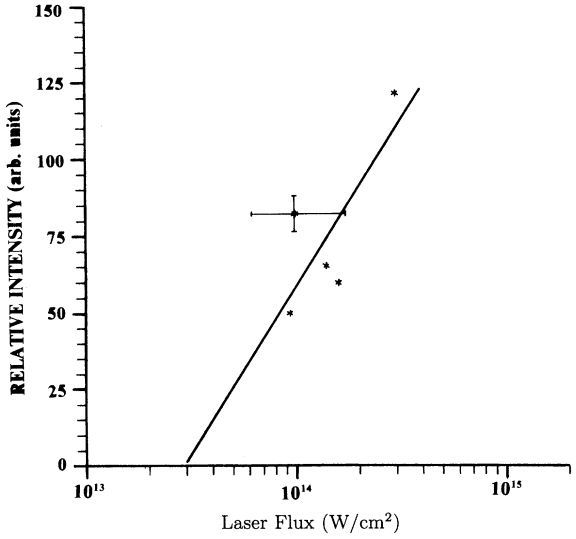

FIG. 4. Experimental determination of the parametric decay instability threshold through its contribution to the second-harmonic generation. The second satellite peak intensity in arbitrary units is drawn as a function of incident laser flux intensity. The observed threshold is equal to 2×10^{13} W/cm^2.

where T (eV) is the electron temperature in electron volts, λ_μ the pump wavelength in μm, and L_μ the density scale length in μm. For typical values of these parameters, where the density scale length is of order of the focal spot diameter, i.e., $L_\mu=22\ \mu$m, and the temperature is taken from some scaling law model [17] as a function of the incident flux, T (eV) $\simeq1$ keV. The theoretical estimate becomes

$$I_{\text{th}}^{\text{PDI}}=1.2\times10^{13}\ \text{W/cm}^2\ .$$

Our experimentally observed value of this threshold is

$$I_{\text{expt}}^{\text{PDI}}=2\times10^{13}\ \text{W/cm}^2\ .$$

This result with the behavior of the second-harmonic intensity peak originating from PDI, as a function of incident flux, is given in Fig. 4.

B. Time evolution of second-harmonic spectra

To construct the evolution of the critical surface velocity, we recorded the spectrum of the harmonic with a time resolution of 0.06 nsec in Fig. 5 (photograph). A

TABLE I. Wavelength shifts of the second harmonic where the secondary peaks are regularly spaced with $2n\omega_{IA}$ frequency difference.

Incident flux (W cm^{-2})	First satellite shift (Å)	Second satellite shift (Å)	Third satellite shift (Å)
9.4×10^{13}	3.0	5.9	8.5
1.08×10^{14}	2.0	4.3	
1.6×10^{14}	2.4	4.1	

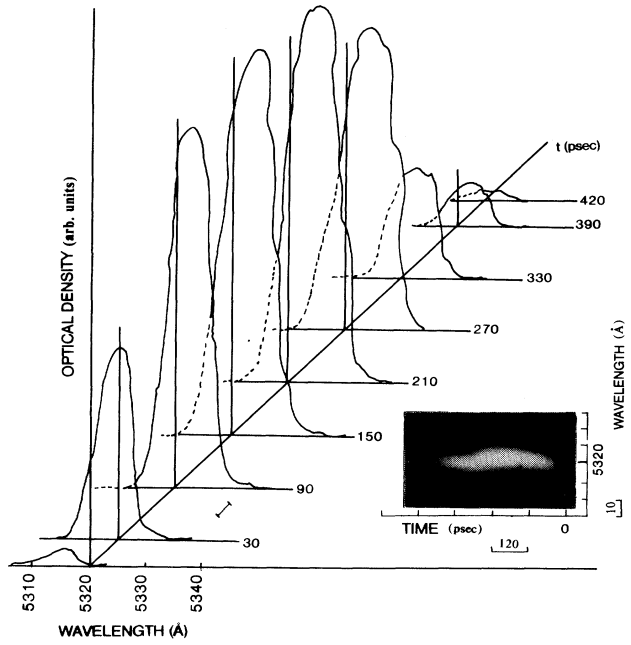

FIG. 5. Second-harmonic optical density time evolution for an incident flux of 4.05×10^{13} W/cm^2. The shifts are observed to switch from blue to red as the critical density velocity changes sign.

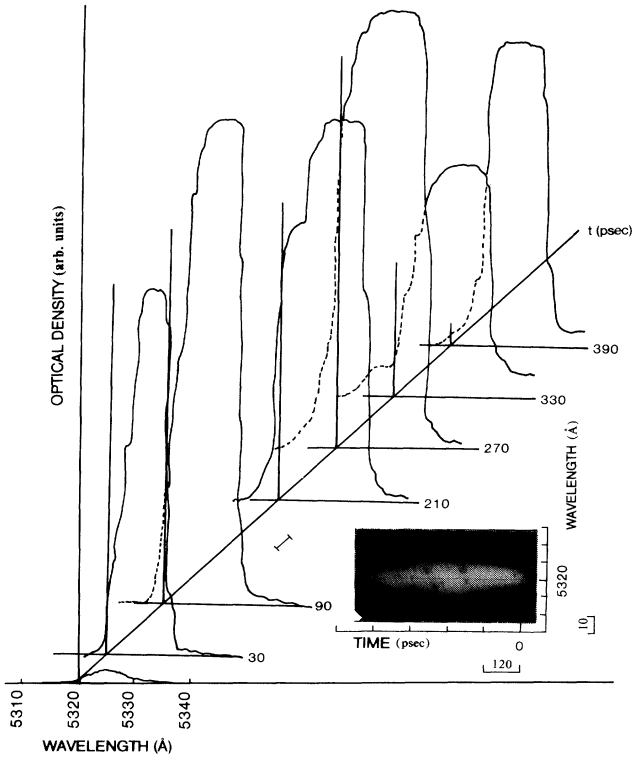

FIG. 6. At an incident flux of 3.0×10^{14} W/cm^2, the optical time evolution of the second harmonic shows an oscillatory behavior attributed to the filamentation of the laser beam. Dark spots on the photograph show the optical density variation due to the plasma-parameter perturbation and its effects on the spatial structure of the laser beam.

typical time scan of the 2ω spectrum is seen and it has been obtained with the aid of a spectrograph and a fast streak camera. In the same figure is also shown the spectral distribution obtained in processing the time scan through a microdensitometer. The wavelength of the main peak of the second harmonic is observed to increase with time. For $t<0.03$ nsec, the spectrum has an increasing blueshifted amplitude as more photons arrive with time to n_c and the Doppler shift indicates the motion of the critical density towards the beam as the plasma starts its expansion.

The velocity of the critical surface can thus be calculated as $u=c\Delta\omega/4\omega_0$, where $\Delta\omega$ is the shift, c the speed of light, and ω_0 the pump frequency (e.g., at $t=0.21$ nsec, $\Delta\lambda=5$ Å, and $u=1.4\times10^7$ cm/s). At $t>0.03$ nsec, the intensity of the second harmonic increases with a stronger red shift. This is the result of the Gaussian laser pulse used, where the bulk of photons arrive at times around 0.27 nsec. Here the Doppler shift indicates that the velocity of the critical surface is directed toward the target in the same direction as the beam.

In Fig. 6 the spectrum of the 2ω is obtained at an incident flux of 3×10^{14} W/cm^2, the highest flux in our experiment. This intensity is above all thresholds of the parametric instabilities. The optical density has been enhanced in comparison to Fig. 5 at an equivalent time. The shifts also indicate that the critical density moves toward the target from the start of the interaction, in the same direction as the beam.

The main feature of the optical-density time evolution is its oscillatory structure, where the peaks experience highs and lows as the Gaussian beam impinges in the inhomogeneous plasma.

In the photograph in Fig. 6, some dark spots are observed, indicating that the critical density surface is presenting a roughness to the arriving photon beam. This large enhancement of harmonic emission is possible because of the formation of electrostatic resonant structure resulting from the modification of the density profile where cavitons are seeded [18]. The incidence of such high intensity flux on a rough critical surface perturbs both ponderomotive and thermal forces, and the laser beam structure will be altered by filamentation. Decomposition of the beam in dense filaments sequentially arising and collapsing, before reaching n_c, creates hot spots in the plasma (Fig. 6, photograph) with temperature increase and density perturbation in the phase-matching zones. Some of the filaments (beamlets) may survive up to n_c, where they arrive as dense light packets with varying intensity and there produce plasmons through resonant absorption.

These, ultimately, recombine to produce second-harmonic light at a varying rate. As a result of such a sequence of plasmon production, we observe in Fig. 6 an oscillatory second-harmonic spectrum. Unstable critical motion and self-focusing of the laser beam have been ob-

served to have a strong effect on the 2ω spectrum [6]. Irregular plasma-parameter variation, such as the temperature and the density scale length, are at the origin of the oscillatory structure of the second harmonic.

IV. DISCUSSION

Observation of burst phenomena of the second-harmonic emission has been reported by several authors [18-23]. Explanations vary from one author to another depending on experimental conditions as well as theoretical hypotheses.

However, most of them do not contradict each other. The various relevant explanations offered to the observations [19] include oscillatory motion of the critical surface driven by the ponderomotive force, modification of the dielectric function of the plasma by a burst of hot electrons generated at the critical surface, and rapid variation in the direction of the emission due to the rippling of the critical surface. However, most of these explanations were, by the authors admitted, rather tentative.

The oscillation of the second-harmonic emission has also been predicted theoretically before [18,2]. The driving mechanism of such emission in a burst is a direct consequence of the fact that in a inhomogeneous plasma, the momentum relation (phase-matching condition) for the process $l+t\rightarrow t$ is fulfilled only locally at the phase-matching point. Erokhin, Moiseev, and Mukhin [2] were the first to show that when the resonance absorption dominates, the second-harmonic emission may oscillate as the electron temperature in the plasma increases. The coalescence of the plasmon with a photon occurs at a distance from the critical surface,

$$d_{2\omega}\simeq 9(v_e/c)^2L \ ,$$

where v_e is the electron thermal velocity, c the speed of light, and L the plasma density scale length near the critical surface. With increasing temperature, it can be shown by using the dispersion relation for longitudinal (Bohm-Gross) and transverse waves, $d_{2\omega}$ increases toward low densities, thereby passing the standing-wave structure of the fundamental transverse wave. When the phase-matching point coincides with a node of the pump field, the second-harmonic intensity will assume a minimum value, whereas in the opposite case it will pass a maximum. In this way high and low values of the second-harmonic intensity will alternate until the longitudinal wave is Landau-damped. Thus the temperature dependence of the second-harmonic intensity is correlated with the spatial structure of the local density and electric-field perturbations which play the decisive role in the generation process. The temperature increase associated with this process is usually attributed to the temporal evolution of the laser pulse as a whole heating the plasma.

In the present experiment, in addition to the oscillation behavior of the second-harmonic intensity, hot spots are observed (Fig 6) and are most probably the major source of the temperature rise. Regarding this subject, Obenschain *et al.*, [7] through use of the technique of induced spatial incoherence (ISI), introduced rapidly changing (on a laser coherence time scale) spatial nonuniformities in the laser coherence time; the would-be nonuniformities average out to produce uniform illumination [24]. By smoothing the beam this way, the effects of the hot spots seeding the self-focusing instability have been suppressed. Before the smoothing ISI technique, correlation of hard x rays with increased second-harmonic emission has been observed [7].

In the experiment conducted here, no smoothing has been used; hence, the laser beam is subject to self-focusing where it develops substructure and collapses into a number of filaments. These filaments become very intense and small. The strong gradients in intensity and density enhance the 2ω emission at first. In the next step ion waves are expected to be generated in the final, nonadiabatic stage of the formation of such intense narrow filaments. These ion waves can provide density modulation which acts to delocalize or spray the filaments [25].

As the beam impinges into the plasma, this sequence of events is reproduced during the pulse width, making the second-harmonic amplitude vary. This is the most probable sequence of events which may explain the oscillatory structure and the presence of hot spots experimentally observed in Fig. 6.

V. CONCLUSIONS

Sideway scattered second-harmonic spectra are experimentally observed to originate from the critical surface laser-plasma-interaction system. Due to the nonlinear processes involved, local plasma parameters are altered by the events. As a consequence of the changes, laser-plasma-interaction physics couples the harmonic generation to laser-beam behavior. it has been observed that the 2ω time-resolved spectrum presents an oscillatory structure due to the formation of unstable filaments. Moreover, the decomposition of the incident beam into intense beamlets is at the origin of the critical surface roughness. Quantification of this effect and the critical surface dynamics may deserve further investigation.

ACKNOWLEDGMENT

The authors wish to thank the Centre de Développement des Téchnologies Avancées for its formal support during the present work.

[1] J. L. Bobin, M. Decroisette, B. Meyer, and Y. Vitel, Phys. Rev. Lett. **30**, 594 (1974).

[2] N. S. Erokhin, S. S. Moiseev, and V. V. Mukhin, Nucl. Fusion **14**, 333 (1974).

[3] N. G. Basov, V. Yu. Bychenkov, O. N. Krokhin, M. V. Osipov, A. A. Rupasov, V. P. Silin, G. V. Sklizkov, A. N. Starodub, V. T. Tikhonchuk, and A. S. Shikanov, Zh. Eksp. Teor. Fiz. **76**, 2094 (1979) [Sov. Phys. JETP **49**, 1059 (1979)].

[4] A. Giulietti, D. Giulietti, D. Batani, V. Biancalana, L. Gizzi, L. Nocera, and E. Schifano, Phys. Rev. Lett. **63**, 524 (1989).

[5] K. Tanaka, W. Seka, L. M. Goldman, M. C. Richardson, R. W. Short, J. M. Soures, and E. A. Williams, Phys. Fluids **27**, 2187 (1984).
[6] Youichi Takada, Noburu Nakano, and Hiroto Kuroda, Phys. Fluids **31**, 692 (1988).
[7] S. P. Obenschain, J. Grun, M. Herbst, K. Kearney, C. Manka, E. McLean, A. Mostovych, J. Stamper, R. Whitlock, S. Bodner, J. Gardner, and R. Lehmberg, Phys. Rev. Lett. **56**, 2807 (1986).
[8] A. J. Schmitt, Phys. Fluids B **3**, 186 (1991).
[9] P. E. Young, H. A. Baldis, T. W. Johnston, W. L. Kruer, and K. G. Estabrook, Phys. Rev. Lett. **63**, 2812 (1989).
[10] A. V. Vinogradov and V. V. Dustovalov, Zh. Eksp. Teor. Fiz. **63**, 940 (1972) [Sov. Phys.—JETP **36**, 492 (1973)].
[11] F. Begay, Phys. Lett. A **153**, 35 (1991).
[12] J. Brilland, L. Berge, A. Gomes, Y. Quemiener, C. Arnas, M. Armengand, J. P. Dinguirard, and D. Pesme, Phys. Fluids B **2**, 160 (1990).
[13] R. Sigel, J. Phys. (Paris) Colloq. **38**, C6-35 (1977).
[14] A. Simon, R. W. Short, E. A. Williams, and T. Dewandre, Phys. Fluids **26**, 3107 (1983).
[15] F. F. Chen, *Introduction to Plasma Physics* (Plenum, New York, 1974), p. 259.
[16] F. W. Perkins and J. Flick, Phys. Fluids **14**, 2012 (1971).
[17] R. Fabbro, C. E. Max, and E. Fabre, Phys. Fluids **28**, 1463 (1985).
[18] N. E. Andreev, G. Auer, K. Baumgartel, and K. Sauer, Phys. Fluids **24**, 1492 (1981).
[19] P. D. Carter, S. M. L. Sim, and T. P. Hughes, Opt. Commun. **27**, 423 (1978).
[20] N. S. Erokhin, V. E. Zakharov, and S. S. Moiseev, Zh. Eksp. Teor. Fiz. **56**, 179 (1969) [Sov. Phys.—JETP **29**, 101 (1969)].
[21] R. A. M. Maddever, B. Luther-Davies, and R. Dragila, Phys. Rev. A **41**, 2154 (1990).
[22] D. R. Gray, J. Murdoch, S. M. L. Sim, A. J. Cole, R. G. Evans, and W. T. Toner, Plasma Phys. **22**, 967 (1980).
[23] K. G. Estabrook, Phys. Fluids **19**, 11 (1976).
[24] R. H. Lehmberg and S. P. Obenschain, Opt. Commun. **46**, 27 (1983).
[25] H. A. Rose, D. F. Dubois, and D. Russel, Fiz. Plazmy **16**, 926 (1990) [Sov. J. Plasma Phys. **16**, 537 (1990)].

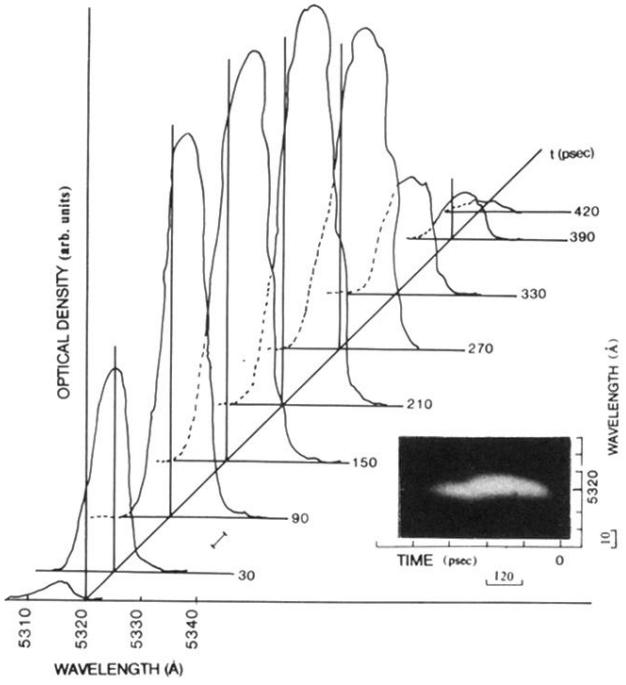

FIG. 5. Second-harmonic optical density time evolution for an incident flux of 4.05×10^{13} W/cm^2. The shifts are observed to switch from blue to red as the critical density velocity changes sign.

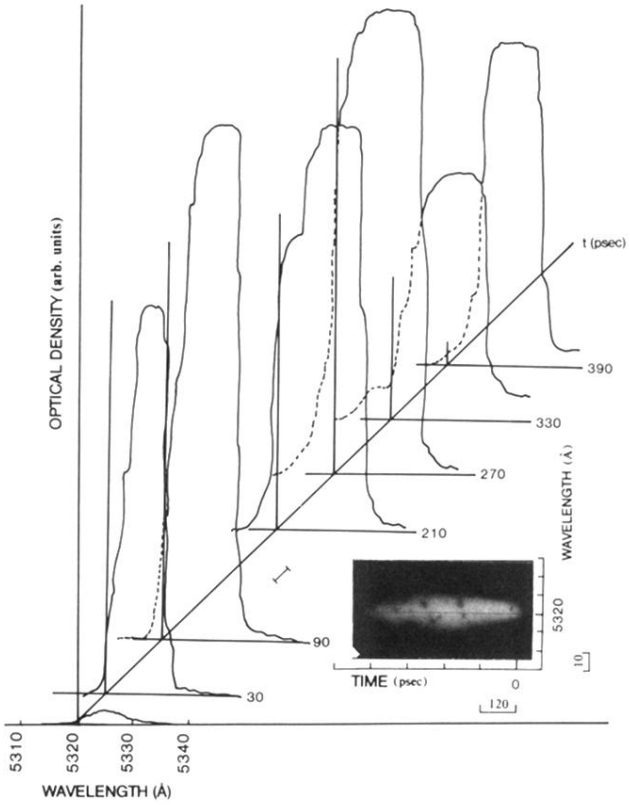

FIG. 6. At an incident flux of 3.0×10^{14} W/cm^2, the optical time evolution of the second harmonic shows an oscillatory behavior attributed to the filamentation of the laser beam. Dark spots on the photograph show the optical density variation due to the plasma-parameter perturbation and its effects on the spatial structure of the laser beam.